Appl Nanosci (2013) 3:263–269
DOI 10.1007/s13204-012-0131-7

ORIGINAL ARTICLE

C_{14}TAB-assisted CeO_2 mesocrystals: self-assembly mechanism and its characterization

N. Krishna Chandar · R. Jayavel

Received: 2 April 2012 / Accepted: 29 April 2012 / Published online: 18 May 2012

Abstract C_{14}TAB-assisted cerium oxide (CeO_2) mesocrystals have been synthesized via wet chemical route. XRD, SEM, AFM, EDS, FTIR, Raman, UV–vis and PL spectroscopy were employed to characterize the crystal phase, morphology, chemical composition and optical properties of the CeO_2 mesocrystals. The experimental results showed that the product owned mesocrystal structure with self-assembly cubic architecture in the presence of C_{14}TAB as a template. The growth mechanism of CeO_2 mesocrystals has been predicted to explain the formation of CeO_2 mesocrystals. CeO_2 mesocrystals exhibit a very strong violet/blue emission centered at 421 nm and a weak green luminescence emission at around 524 nm.

Keywords Mesocrystals · C_{14}TAB · AFM · Self-assembly

Introduction

Cerium oxide (CeO_2) is one of the most important rare earth materials due to its wide applications as oxygen sensors, fuel cells, UV absorbents and filters, buffer layers with silicon wafer, catalysts, optical devices and polishing materials (Bumajdad et al. 2009; Lawrence et al. 2011). CeO_2 with varying morphologies like nanorods, nanocubes, nanotubes, nanoplates, triangular and rhombic microplates, nanowires have been successfully synthesized, most of which possessed polycrystalline or single-crystalline structures (Ho et al. 2005; Lin and Chowdhury 2010; Mai et al. 2005). Hence, it is well documented that the shape and size of nanostructures can control their widely changing optoelectronic and chemical properties.

Mesocrystals have received rapidly increasing attention since they were first proposed as a new class of ordered nanoparticle superstructures by Cölfen and Mann (2003). A mesocrystal is a quasi-single-crystal consisting of ordered assemblies of small, anisotropic, and vectorially aligned nanoparticles, thus forming an entirely new class of porous metamaterials through mesoscopic transformations and nano-particle precursors. This system has drawn much attention, because it is of importance for many fascinating phenomena, such as fabricating nanostructured devices. As intermediates, mesocrystals can be good supplements to polycrystals and single crystals because of the strong interaction among their ordered units and the size can be tuned by controlling the bottom-up growth conditions. Mesocrystals not only maintain the properties of nanoparticles in microscale but can even exhibit unique characteristics or improved properties. The structure and properties of mesocrystals are inseparably related to their size and the way the assembly units are attached. This suggests that it is possible to achieve various advanced properties by controlling the structures of mesocrystals.

Mo et al. (2008) synthesized mesocrystal ZnO microtubules, providing fundamental model systems to load noble metal nanoparticles for catalytic and electro catalytic applications. Li et al. (2011) synthesized hollow zinc oxide mesocrystals, useful for catalytic applications. Ye et al. (2011) fabricated large scale tunable anatase TiO_2 mesocrystals for energy and environmental applications. Yuejnan et al. (2007) produced high surface area nano-CeO_2 particles from $Ce(NO_3)_3$ and NaOH as precipitation agent

N. Krishna Chandar · R. Jayavel (✉)
Centre for Nanoscience and Technology,
Anna University, Chennai 600025, India
e-mail: rjvel@annauniv.edu

N. Krishna Chandar
e-mail: nkchandar@gmail.com

using CTAB used as template. Lu et al. (2009) employed hydrothermal route to fabricate prism-like mesocrystal CeO_2. A facile β-cyclodextrin-assisted hydrothermal method was used by Xue et al. (2011) to prepare hierarchical walnut-like $CeOHCO_3$ and CeO_2 mesocrystals. Wang et al. (2011) employed surfactant free non-aqueous synthesis route using $Ce(NO_3)_3$ and octanol as the reactants at a reaction temperature of 150 °C to prepare uniform quasi-octahedral CeO_2 mesocrystals.

However, to the best of our knowledge, there have been few reports on the synthesis and property studies of CeO_2 mesocrystals. The present investigation describes the wet chemical synthesis and self-assembly mechanism of CeO_2 mesocrystals using tetradecyltrimethyl ammonium bromide C_{14}TAB (Borodko et al. 2009) as a template. The prepared CeO_2 mesocrystals were characterized by XRD, SEM, AFM, EDS, FTIR, Raman, UV–vis and PL studies.

Experimental

Materials synthesis

Analytical-grade cerium nitrate hexahydrate (0.0375 M) and C_{14}TAB were dissolved in 25 ml of Millipore water (18 MΩ). Aqueous ammonium hydroxide solution was added drop wise to the above solution to achieve the pH of ~9. After constant stirring at room temperature, the pale-yellow precipitated powders were collected and washed with anhydrous ethanol and water to remove the ionic impurities. The purified particles were dried at 120 °C in air for 24 h, which resulted in the formation of CeO_2 mesocrystals.

Materials characterization

XRD analysis was carried out with Cu K_α radiation ($\lambda = 1.5406$ Å) using a Bruker D8 diffractometer with the scanning rate of 0.05° s^{-1} in the 2θ range from 10° to 70°. SEM and EDS was obtained with HITACHI S-3700 N scanning electron microscope with accelerating voltage of 20 kV. AFM was imaged with XE-70 Park Instruments using non-contact operation mode. TG–DTA analysis was carried out with a SII TG/DTA 6300 EXSTAR apparatus with a heating rate of 10 °C min^{-1} under flowing air. FTIR spectrum was recorded using a Perkin-Elmer Spectrum One spectrometer in the 400–4,000 cm^{-1} range at a resolution of 4 cm^{-1}. Raman spectrum was collected using a Bruker SENTERRA Raman spectrometer with excitation source of 785 nm YAG laser in the range 800–100 cm^{-1} with the spectral resolution of 1 cm^{-1}. The UV–vis spectrum was recorded using T90+ UV/VIS spectrophotometer at room temperature in the wavelength range between 200 and 800 nm. The photoluminescence was recorded using a Jobin–Yvon Fluorolog-3-TAU steady-state/lifetime spectrofluorometer in range 400–650 nm.

Results and discussion

Structural analysis

Crystalline phases of the prepared CeO_2 mesocrystals were examined by XRD analysis. All diffraction peaks in Fig. 1 have been indexed to cubic fluorite structure of CeO_2 (space group: *Fm3m*). The intensive diffraction peak located at $2\theta = 28.41°$ is from the (1 1 1) lattice plane of fcc CeO_2. No impurity peaks were observed, revealing high purity of the sample. The calculated lattice constant (Table 1) based on the six distinct peaks is consistent with standard data for CeO_2 (JCPDS 34-0394) and also with earlier reports (Shih et al. 2010; Sujana et al. 2008).

Morphological studies

The SEM images obtained from CeO_2 mesocrystals are shown in Fig. 2. Figure 2a shows that the product consists of a large quantity of cube-like mesocrystals with a narrow size distribution. Moreover, the SEM image depicts that an individual CeO_2 mesocrystal is pointed, as shown in Fig. 2b.

Figure 3 demonstrates the morphology of CeO_2 mesocrystals imaged through AFM. It is clearly observed from Fig. 3a–c that the particles in nano regime are attached together to form aligned nanoplates, arranged with almost the same orientation, which are composed of a cubic crystal, termed as mesocrystal. The cubes that form the mesostructures have corroded edges and corrugated surfaces. The crystals are composed of nanoscale building units, oriented along the principal axis of the particle, revealing

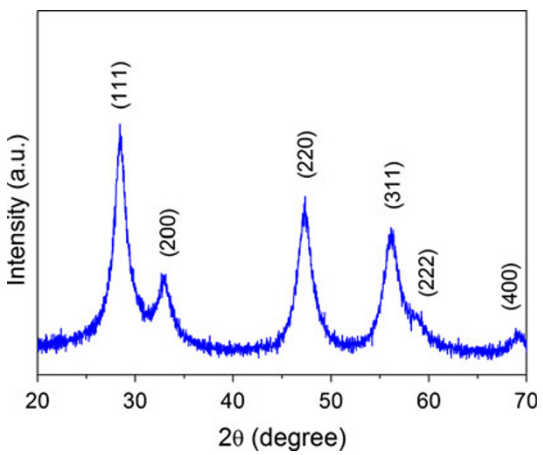

Fig. 1 XRD pattern of the CeO_2 mesocrystals

Table 1 Calculated lattice constant of C_{14}TAB-assisted CeO_2 mesocrystals

Sample	h k l	*d* spacing		Lattice constant *a* (nm)
		(calc)	(exp)	
CeO_2 mesocrystals	1 1 1	3.124 (0)	3.138 (7)	0.5421
	2 0 0	2.705 (5)	2.717 (0)	
	2 2 0	1.913 (0)	1.921 (9)	
	3 1 1	1.631 (4)	1.640 (7)	
	2 2 2	1.562 (0)	1.571 (7)	
	4 0 0	1.352 (7)	1.362 (3)	

that the lateral and basal faces of the precipitate are composed of stacked nanoparticle layers with a thickness between 30 and 40 nm. It is observed that the nanoplates can self-assemble, forming a cubic architecture along the longitudinal and horizontal axes in the presence of C_{14}TAB as template. The line-profile plot (Fig. 3d) depicts that the mean diameter and length of the crystals are about 350 and 450 nm, respectively. No impurities were detected for the CeO_2 mesocrystals in EDS analysis (Fig. 4), indicating that pure CeO_2 mesocrystals are formed.

Thermal analysis

TG/DTA curves of CeO_2 powders are shown in Fig. 5. The TG curve exhibits two distinct weight-loss steps: the first weight-loss step ~4 % between ~30 and 200 °C, indicating that it is slightly hydrated. These weight losses are related to the loss of moisture and trapped solvent. The second dramatic weight-loss step (~16 %) between ~200 and 300 °C is due to the combustion of organic residues. No considerable weight loss was observed above 460 °C, suggesting the formation of crystalline CeO_2 as a decomposition product. The DTA curve shows a strong exothermic peak at 265 °C and minor peak at 295 °C, correlated to a weight loss confirming the combustion of organic residues due to the crystallization of residual amorphous phase.

FTIR analysis

Figure 6 shows the FTIR spectrum of the CeO_2 mesocrystals. The intense absorption band at 3,444 cm^{-1} corresponds to the O–H mode of (H–bonded) water molecules. There are peaks at 2,918 and 2,846 cm^{-1}, corresponding to the asymmetric and symmetric stretching vibrations of C–CH_2 in the methylene chains. The sharp peaks at 1,630 and 1,450 cm^{-1} are specified as the deformation of –CH_2 and –CH_3 symmetric stretching vibrations of the surfactant. In addition to this, the bands observed at 1,384, 1,095, 1,047, 873, 817 and 780 cm^{-1} are assigned to CO_3^{2-} vibrations of C_{14}TAB surfactant (Wang et al. 2009). The doublet peaks at 736 and 710 cm^{-1} correspond to the rocking mode of methylene chain, indicating that methylene chains of C_{14}TAB were packed to form restricted structures. The spectrum also exhibits a broad band at 524 cm^{-1} which is due to the Ce–O mode (inset of Fig. 6). These results indicate that the surfactant C_{14}TAB is used as a template for constructing the building block of mesocrystals, which is also in good agreement with the result of TG/DTA.

Raman spectral analysis

The formation of a cubic structure of CeO_2 sample is further supported by Raman spectroscopy. Figure 7 shows a typical Raman spectrum of CeO_2 mesocrystals. The broad peak of Raman spectrum is mainly due to the stretching vibrations of CeO_2 nanoparticles which is the building block for the formation of mesocrystals. The Raman-active mode for the CeO_2 sample is 461.04 cm^{-1}, which is attributed to F_{2g} symmetrical breathing mode O atoms around the each cerium ions. Since only the O atoms move, the vibrational mode is nearly independent of the ionic mass of cerium (Zhang et al. 2002).

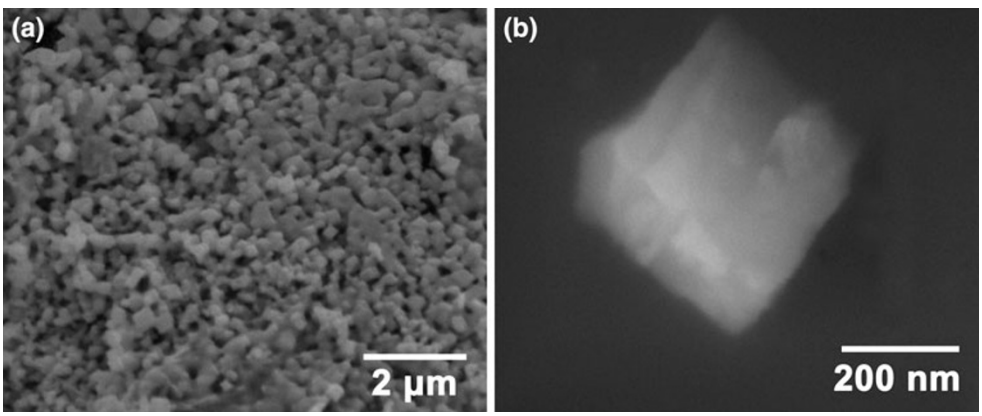

Fig. 2 **a** SEM image of CeO_2 mesocrystals, **b** SEM image of an individual CeO_2 mesocrystal

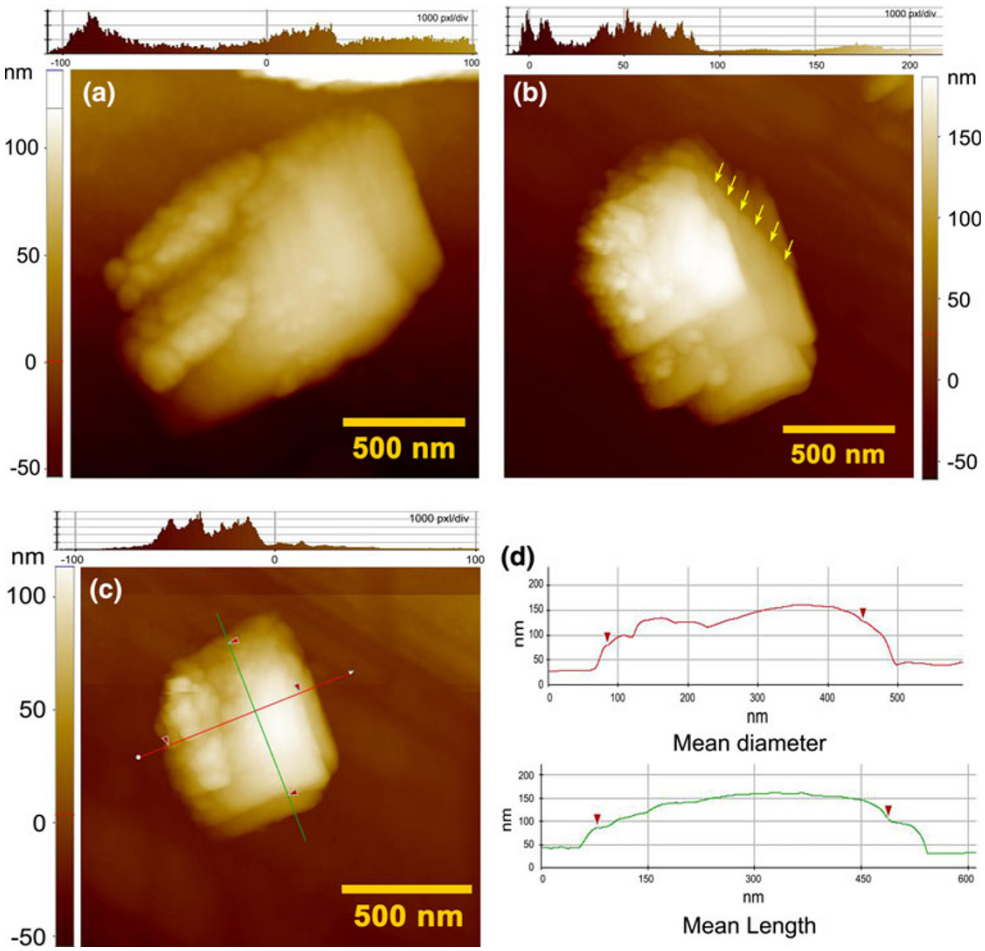

Fig. 3 **a**, **b** AFM images revealing details of self-assembly nanoparticle layers arranged on almost the same orientation, indicating with *arrow mark*, **c** AFM image revealing the dimension determination, **d** *line-profile plot* depicts the mean diameter and length of the CeO_2 mesocrystals

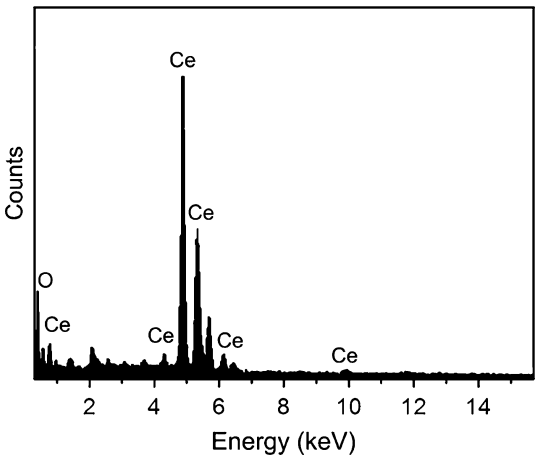

Fig. 4 EDS spectrum of CeO_2 mesocrystals

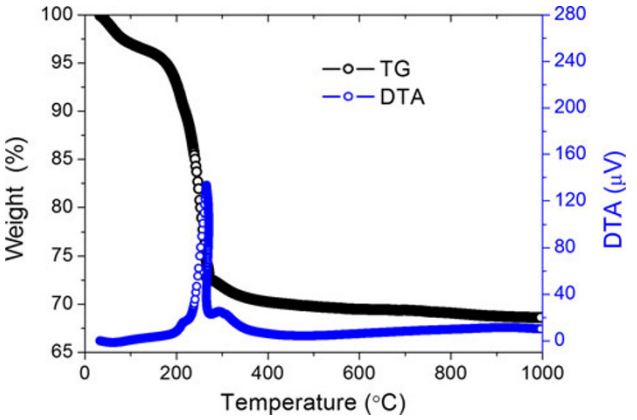

Fig. 5 TG/DTA curves of thermal decomposition of the CeO_2 mesocrystals at a heating rate of 10 °C min^{-1} in static air

Formation mechanism for CeO_2 mesocrystals

Based on the above results, the formation mechanism of the CeO_2 mesocrystals is proposed. The possible chemical reaction for the synthesis of CeO_2 mesocrystals can be expressed as,

$$Ce(NO_3)_3 \cdot 6H_2O_{(aq)} \rightarrow Ce^{4+}_{(aq)} + 3NO^-_3 + 6H_2O \quad (1)$$

$$Ce^{4+}_{(aq)} + 4OH^-_{(aq)} \xrightarrow{C_{14}TA^+} Ce(OH)_{4(s)} \quad (2)$$

$$Ce(OH)_{4(s)} \xrightarrow{O_2} CeO_{2(s)} + 2H_2O \quad (3)$$

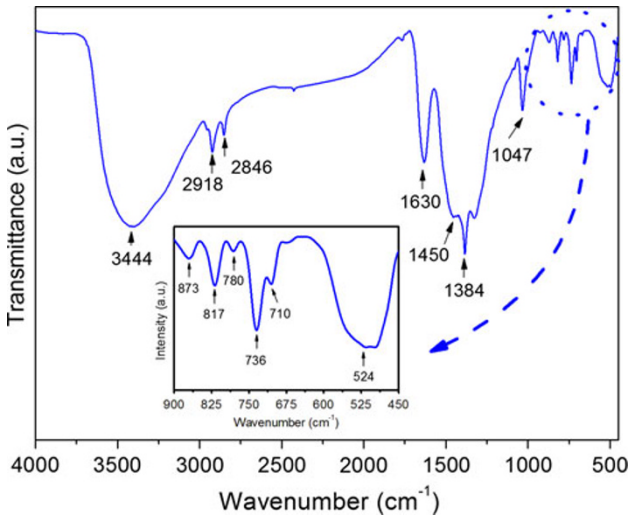

Fig. 6 FTIR spectrum of CeO_2 mesocrystals

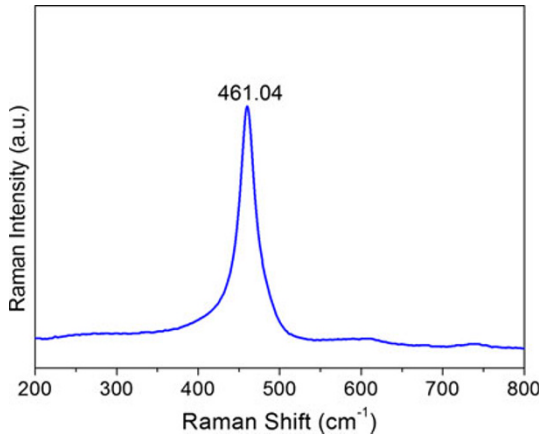

Fig. 7 Raman spectrum of CeO_2 mesocrystals

Under basic conditions, $Ce(NO_3)_3{\cdot}6H_2O$ decomposes to form Ce^{4+} along with its byproducts as shown in Eq. (1). It is known that the basic medium is favorable for the formation of Ce^{4+} ion (Sun et al. 2005). The OH^- in the base reactant reacts with the acid reactant of Ce^{4+} in the solution, resulting in homogeneous precipitation. Simultaneously, the surfactant C_{14}TAB molecules dissociated to form $C_{14}TA^+$ in the basic aqueous solution. As per Eq. (2), $Ce(OH)_4$ is formed through the hydrolysis of Ce^{4+} in the presence of $C_{14}TA^+$ followed by the oxidation of O_2 from air to form CeO_2 (Eq. 3). It is observed that C_{14}TAB plays a key role in the formation of CeO_2 mesocrystals. The CeO_2 nanoparticles, which are directed by specific organic additives, can act as the basic building units to assemble into mesocrystals.

Schematic representation of a tentative self-assembly growth mechanism for the formation of CeO_2 mesocrystals is proposed in Fig. 8. The main pathways of crystallization involve the arrangement of primary nanoparticles into an iso-oriented crystal via self-assembly process in the presence of structure-directing template; finally, forming a well-defined crystal upon aggregation of the nanoparticles. Aggregation of nanoparticles is a very common phenomenon since the nanoparticles tend to decrease the exposed surface to lower the surface energy. In principle, when two particles are in contact, likely they tend to rotate with each other to minimize the interface strain energy. Therefore, same type of crystal planes tends to align with each other, forming a coherent interface with decreasing interfacial energy (Cölfen and Mann 2003). When the pH reaches 9, the solution involves abundant OH^- ions, which consequently has much higher nucleation rate due to the existence more nucleus clusters in solution. However, crystal growth rate is inhibited, leading that the small crystals aggregate randomly oriented along epitaxial direction, which form CeO_2 mesocrystals (Lu et al. 2009). Nevertheless, the formation mechanism of CeO_2 mesocrystals needs further investigation.

UV–vis spectral analysis

The effect of surface adsorbing species on the optical properties of CeO_2 mesocrystals was examined by UV–vis spectral analysis. Figure 9 shows the UV–visible absorption spectrum of CeO_2 mesocrystals. The spectrum shows a strong absorption below 400 nm with a well-defined absorbance peak at around 320 nm. The optical band gap E_g for a semiconductor can be determined from the Eq. (4).

$$ahv = A(hv - E_g)^{1/n} \quad (4)$$

where h is the photon energy, α is the absorption coefficient, A is a constant relative to the material, and n is 2 for a direct transition. The plot of $(\alpha hv)^2$ versus photon energy for the sample is shown as inset in Fig. 9. It reveals that the band gap of CeO_2 mesocrystals is about 3.77 eV, which is greater than the value for the bulk CeO_2 ($E_g = 3.19$ eV) (Zhang et al. 2009). The blue shifting of the band gap is due to quantum size effect, which results from the smaller size of primary CeO_2 nanoparticles constructing the CeO_2 mesocrystals. As a result, quantum size effects will increase the band gap leading to a blue shift in the absorption spectrum. Similar results are observed by Wang et al. (2011) for their quasi-octahedral CeO_2 mesocrystals.

Photoluminescence studies

The PL spectrum of CeO_2 mesocrystals with the excitation wavelength of 350 nm is shown in Fig. 10. The violet/blue light emission peak at 421 nm could be explained by charge transition from the 4*f* band to the valence band of CeO_2. It is easy to observe the hopping from Ce 4*f* to O 2*p* (>3 eV). In addition, the defect levels localized between the Ce 4*f* band

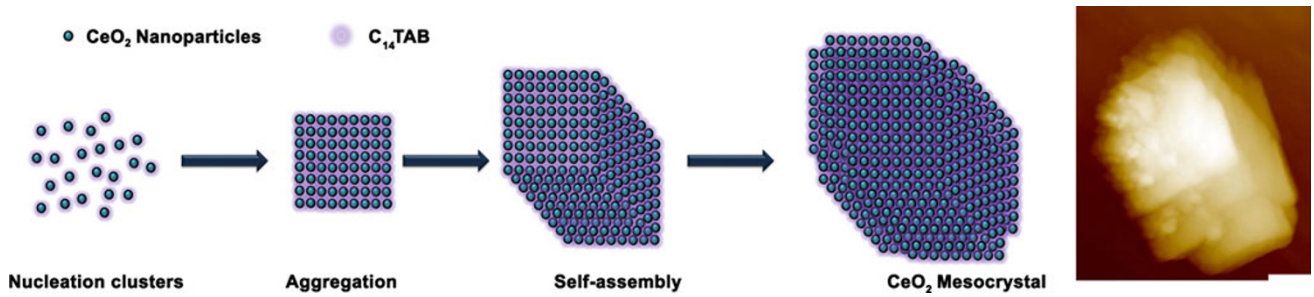

Fig. 8 Schematic representation of a tentative self-assembly growth mechanism for the formation of CeO_2 mesocrystals

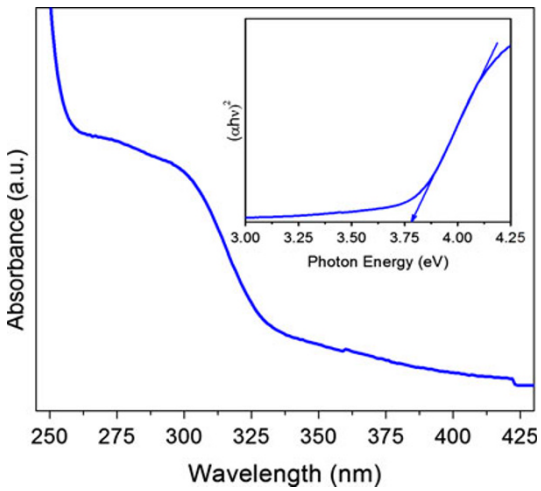

Fig. 9 UV–vis absorption spectrum of CeO_2 mesocrystals. The *inset* shows the plot of $(\alpha hv)^2$ as a function of photon energy for the CeO_2 mesocrystals

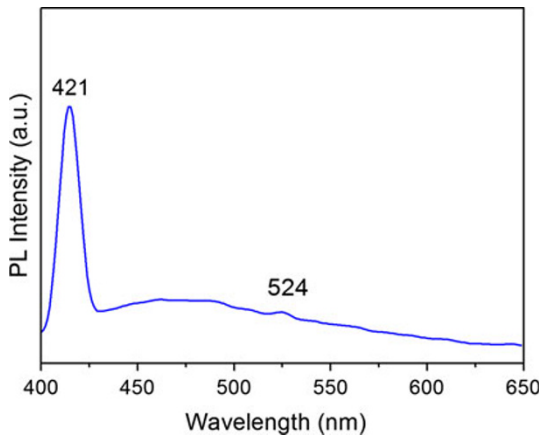

Fig. 10 Photoluminescence spectra of CeO_2 mesocrystals taken with the excitation wavelength of 350 nm

and the O 2*p* band can result in wider emission bands. The other green emission peak centered at 524 nm is attributed to the surface vacancies (Chen et al. 2007). Since the CeO_2 mesocrystals have specific oriented aggregation of individual nanoparticles, there are numerous internal boundaries and surfaces, where defects exist and decrease the recombination energy of electrons and holes. Compared with the absorption and emission spectra, the observed blue shift could be attributed to the quantum confinement effect of nanoparticles in the CeO_2 mesocrystals. As a whole, the change in the optical properties of CeO_2 mesocrystals is ascribed to the effect of surfactant $C_{14}TAB$ on the band structures of CeO_2 nanoparticles. It has further impacted the electronic transitions, giving rise to particle growth behavior and the concomitant presence of low valence ions (Gu and Soucek 2007; Phoka et al. 2009).

Conclusions

CeO_2 mesocrystals were synthesized using $C_{14}TAB$ as a surfactant by wet chemical synthesis route. The XRD pattern confirmed the formation of phase pure CeO_2 mesocrystals with cubic fluorite structure. The SEM and AFM images showed the morphology of cubic architecture of CeO_2 mesocrystals with mean diameter and length of about 350 and 450 nm, respectively. The TG/DTA and FTIR results clearly indicated that the surface of the CeO_2 nanoparticles was chemically bonded with the surfactant. A possible formation mechanism of CeO_2 mesocrystals is proposed on account of aggregation of nanoparticles along with the epitaxial orientation. The UV–vis spectrum showed a blue shift with a band gap $E_g = 3.77$ eV, which was attributed to the quantum confinement effect of nanoparticles present in the CeO_2 mesocrystals. The sample also exhibited photoluminescence of violet/blue light at 421 nm and a weak green luminescence emission at around 524 nm. Because of its unique structure and properties, the prepared CeO_2 mesocrystals may be used as sensors and optoelectronic applications.

Acknowledgments One of the authors NKC would like to thank the All India Council for Technical Education (AICTE), Govt of India for awarding the National Doctoral Fellowship (NDF). The characterization facilities provided by SAIF, IITM, Chennai and STIC, CUSAT, Cochin are gratefully acknowledged.

References

Borodko Y, Jones L, Lee H et al (2009) Spectroscopic study of tetradecyltrimethylammonium bromide Pt-C_{14}TAB nanoparticles: structure and stability. Langmuir 25:6665–6671. doi:10.1021/la803406p

Bumajdad A, Eastoe J, Mathew A (2009) Cerium oxide nanoparticles prepared in self-assembled systems. Adv Colloid Interf Sci 147–148:56–66. doi:10.1016/j.cis.2008.10.004

Chen M, Zu X, Xiang X, Zhang H (2007) Effects of ion irradiation and annealing on optical and structural properties of CeO_2 films on sapphire. Phys B 389:263–268. doi:10.1016/j.physb.2006.06.162

Cölfen H, Mann S (2003) Higher-order organization by mesoscale self-assembly and transformation of hybrid nanostructures. Angew Chemie 42:2350–2365. doi:10.1002/anie.200200562

Gu H, Soucek MD (2007) Preparation and characterization of monodisperse cerium oxide nanoparticles in hydrocarbon solvents. Chem Mater 19:1103–1110. doi:10.1021/cm061332r

Ho C, Yu JC, Kwong T, et al (2005) Morphology-controllable synthesis of mesoporous CeO_2 nano- and microstructures. Chem Mater 17(17):4514–4522

Lawrence NJ, Brewer JR, Wang L et al (2011) Defect engineering in cubic cerium oxide nanostructures for catalytic oxidation. Nano Lett 11:2666–2671

Li H, Zhang Y, Liu H, Wang J (2011) Large ZnO mesocrystals of hexagonal columnar morphology derived from liquid crystal templates. J Am Ceram Soc 94:3267–3275. doi:10.1111/j.1551-2916.2011.04498.x

Lin K-S, Chowdhury S (2010) Synthesis, characterization, and application of 1-D cerium oxide nanomaterials: a review. Int J Mol Sci 11:3226–3251. doi:10.3390/ijms11093226

Lu X, Li X, Chen F et al (2009) Hydrothermal synthesis of prism-like mesocrystal CeO_2. J Alloy Compd 476:958–962. doi:10.1016/j.jallcom.2008.09.198

Mai H-X, Sun L-D, Zhang Y-W et al (2005) Shape-selective synthesis and oxygen storage behavior of ceria nanopolyhedra, nanorods, and nanocubes. J Phys Chem B 109:24380–24385

Mo BM-S, Lim SH, Mai Y-W et al (2008) In situ self-assembly of thin ZnO nanoplatelets into hierarchical mesocrystal microtubules with surface grafting of nanorods: a general strategy towards hollow mesocrystal structures. Adv Mater 20:339–342. doi:10.1002/adma.200701137

Phoka S, Laokul P, Swatsitang E et al (2009) Synthesis, structural and optical properties of CeO_2 nanoparticles synthesized by a simple polyvinyl pyrrolidone (PVP) solution route. Mater Chem Phys 115:423–428. doi:10.1016/j.matchemphys.2008.12.031

Shih CJ, Chen YJ, Hon MH (2010) Synthesis and crystal kinetics of cerium oxide nanocrystallites prepared by co-precipitation process. Mater Chem Phys 121:99–102. doi:10.1016/j.matchemphys.2010.01.001

Sujana MG, Chattopadyay KK, Anand S (2008) Characterization and optical properties of nano-ceria synthesized by surfactant-mediated precipitation technique in mixed solvent system. Appl Surf Sci 254:7405–7409. doi:10.1016/j.apsusc.2008.05.341

Sun C, Li H, Zhang H et al (2005) Controlled synthesis of CeO_2 nanorods by a solvothermal method. Nanotechnology 1454:1454–1463. doi:10.1088/0957-4484/16/9/006

Wang S, Xu H, Qian L et al (2009) CTAB-assisted synthesis and photocatalytic property of CuO hollow microspheres. J Solid State Chem 182:1088–1093. doi:10.1016/j.jssc.2009.01.042

Wang X, Ma Y, Sugunan A et al (2011) Synthesis of uniform quasi-octahedral CeO_2 mesocrystals via a surfactant-free route. J Nanoparticle Res 13:5879–5885. doi:10.1007/s11051-011-0416-x

Xue B, Liu R, Xu Z-D (2011) β-Cyclodextrin-assisted preparation of hierarchical walnut-like $CeOHCO_3$ and CeO_2 mesocrystals. Mater Sci Eng B 176:210–216. doi:10.1016/j.mseb.2010.11.009

Ye J, Liu W, Cai J et al (2011) Nanoporous anatase TiO_2 mesocrystals: additive-free synthesis, remarkable crystalline-phase stability, and improved lithium insertion behavior. J Am Chem Soc 133:933–940

Yuejuan W, Jingmeng M, Mengfei L et al (2007) Preparation of high-surface area nano-CeO_2 by template-assisted precipitation method. J Rare Earth 25:58–62. doi:10.1016/S1002-0721(07)60045-3

Zhang Q, Yu Z, Li G et al (2009) Synthesis of quantum-size cerium oxide nanocrystallites by a novel homogeneous precipitation method. J Alloy Compd 477:81–84. doi:10.1016/j.jallcom.2008.10.059

Zhang F, Chan S, Spanier JE et al (2002) Cerium oxide nanoparticles: size-selective formation and structure analysis. Appl Phys Lett 80:127–129. doi:10.1063/1.1430502